Journal of Materials Chemistry A

PAPER

View Article Online
View Journal | View Issue

Cite this: J. Mater. Chem. A, 2016, 4, 12289

High-performance all-solid-state asymmetric stretchable supercapacitors based on wrinkled MnO_2/CNT and Fe_2O_3/CNT macrofilms

Taoli Gu and Bingqing Wei*

Received 6th June 2016
Accepted 5th July 2016

DOI: 10.1039/c6ta04712b

www.rsc.org/MaterialsA

High-performance stretchable energy storage devices are urgently needed due to the rapid development of portable, wearable, and stretchable electronics. However, most of the stretchable single-cell energy storage devices suffer from a relatively low operating voltage and thus a low energy density. Here, we report an all-solid-state asymmetric stretchable supercapacitor (ASS) with high energy density using the wrinkled manganese dioxide (MnO_2)/carbon nanotube (CNT) hybrid film as a positive electrode and the wrinkled iron oxide (Fe_2O_3)/CNT composite film as a negative electrode in a neutral Na_2SO_4–poly(vinyl alcohol) (Na_2SO_4/PVA) gel electrolyte. Due to the high specific capacitance and excellent rate performance of MnO_2/CNTs and Fe_2O_3/CNTs, as well as the synergistic effects of the two electrodes with an optimized potential window, the asymmetric stretchable cell exhibits superior electrochemical and mechanical performances. An optimized ASS can be reversibly cycled in the voltage window between 0 and 2 V, and shows a supreme energy density of 45.8 W h kg^{-1} (corresponding power density of 0.41 kW kg^{-1}). Additionally, the ASS also exhibits exceptional cycling stability and durability, with 98.9% specific capacitance retained even after 10 000 electrochemical cycles at multiple strains. These encouraging results show its great potential in developing stretchable energy storage devices with high energy and power densities for wearable and implantable electronic applications.

Introduction

Along with the rapid development of flexible electronics, stretchable electronics are springing up as a new technological advancement due to their reversible stretchability while still maintaining their functionality.[1–4] Stretchability represents a rigorous challenge of mechanical stability. Stretchable devices must bear large strain deformation and significant shape deformation, including bending, twisting, stretching, *etc.* Therefore, stretchable energy storage devices are strongly desired to power the stretchable electronics.[5–10] However, such stretchable electrochemical double layer supercapacitors (EDLCs) or pseudocapacitors still suffer from low specific capacitance and low working potentials (usually less than 1 V), leading to unsatisfactory energy and power densities, preventing them from usable applications. Therefore, it is imperative to develop a valid approach to enhance their electrochemical performance, while maintaining their high mechanical stretchability.

The asymmetric electrode configuration, taking advantage of the pseudocapacitive positive electrodes to improve the specific capacitance as well as the carbon-based negative electrodes to extend the operating potential, has been demonstrated as an effective way for improving the supercapacitor electrochemical performance.[11–14] The higher operating voltage can not only enhance the energy density but also reduce the number of capacitors in series to achieve an expected output voltage. Lately, the asymmetric electrode configuration has been applied to the newly emerged flexible supercapacitors, such as manganese dioxide (MnO_2)//carbon or graphene,[12–14] graphene//carbon nanotubes (CNTs),[15] graphene–ruthenium oxide (RuO_2)//graphene,[11,16] and graphene–nickel(II) hydroxide ($Ni(OH)_2$)//graphene,[17] but most of these flexible asymmetric supercapacitor prototypes are only capable of bending but not stretching. The simple bendability sustaining the induced strains $\leq 1\%$ is far insufficient for practical applications where the devices would experience more complicated and challenging stretching, which must accommodate large strain deformation $\gg 1\%$.

Transition metal oxides (MeO_x) dominate the pseudocapacitive materials for electrochemical energy storage. As an example, MnO_2 has significant predominance such as abundance, low cost, and a high theoretical specific capacitance (1370 F g^{-1}).[18] Iron oxide (Fe_2O_3) has the advantage of low cost and environmental harmlessness and shows a superior electrochemical performance in negative potentials.[19] Therefore, asymmetric supercapacitors composed of MnO_2 as the positive electrode and Fe_2O_3 as the negative electrode will become a promising energy storage candidate that possesses more economical and environmental superiority. Besides, the redox

Department of Mechanical Engineering, University of Delaware, Newark, DE, 19716, USA. E-mail: weib@udel.edu

reaction process of the typical pseudocapacitive materials has been found to be extremely fast owing to the strong bonded, inherently superior conductive, and porous CNT films.[9] In light of this, different from using sole carbon-based materials as a negative electrode in previously reported asymmetric supercapacitors,[12–17] we focused on enhancing the specific capacitance and energy density of asymmetric supercapacitors using metal oxide electrodes in both electrodes in this work.

Herein, an asymmetric stretchable supercapacitor (ASS) with the MnO_2/CNT hybrid film as the positive electrode, the Fe_2O_3/CNT composite film as the negative electrode, and the Na_2SO_4–poly(vinyl alcohol) (Na_2SO_4/PVA) gel electrolyte has been fabricated. The ASS cell with a stretchability of up to 100% possesses a high potential window of 2 V, a high energy density (45.8 W h kg^{-1}), and high electrochemical and mechanical cycling stability. To the best of our knowledge, this is the first report on a novel asymmetric stretchable energy storage system based on two MeO_x/CNT electrodes, which shows simultaneously excellent electrochemical performance and high stretchability.

Results and discussion

To fabricate the ASS cell, the MnO_2/CNT film, Fe_2O_3/CNT film, and Na_2SO_4/PVA gel electrolyte were used as the positive electrode, negative electrode, and electrolyte, respectively (Fig. 1a). The ASS was made stretchable by applying a simple pre-straining-then-buckling strategy.[5,6] Materials synthesis and cell assembly procedures are depicted in detail in the Experimental section. In brief, a custom-made, two-way movable stage was utilized to pre-stretch a polydimethylsiloxane (PDMS) substrate (with 100% pre-strain); the freestanding MnO_2/CNT and Fe_2O_3/CNT films were then attached and secured to the PDMS substrate, respectively. Subsequently, a liquid Na_2SO_4/PVA gel electrolyte was coated on the surface of electrodes by means of dip coating. After the electrolyte had solidified, two electrodes were stacked together with each other with the electrolyte-coated parts overlapping. Finally, the pre-strain was released to its original length to form the "wrinkled" structure. The SEM figures of the wrinkled MnO_2/CNT and Fe_2O_3/CNT films are shown in Fig. 1b and c, respectively. The precipitated MnO_2 particles and as-synthesized Fe_2O_3 particles were demonstrated to possess nanoscale architectures and evenly distributed within CNT bundles (Fig. 1d and e).

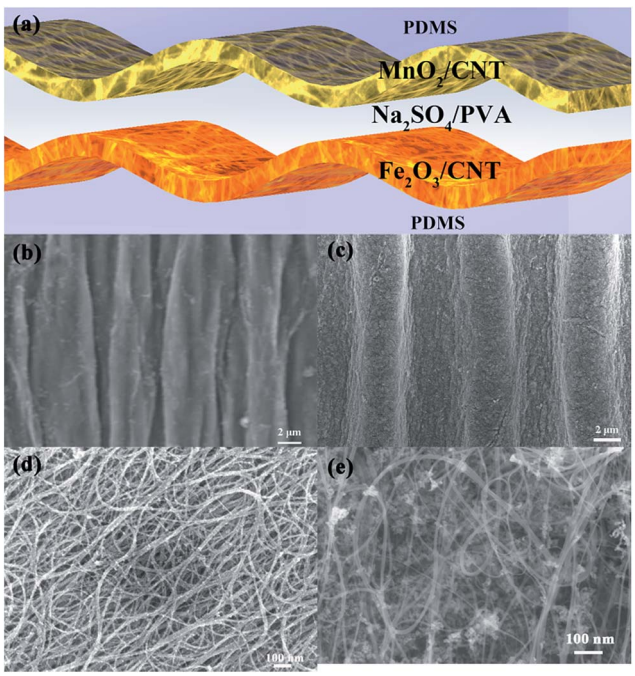

Fig. 1 (a) Schematic illustration of the fabricated ASS cell based on the wrinkled MnO_2/CNT hybrid film as a positive electrode and Fe_2O_3/CNT hybrid film as a negative electrode; SEM image of the wrinkled MnO_2/CNT film (b) and Fe_2O_3/CNT film (c). Magnified SEM image of the MnO_2/CNT film (d) and Fe_2O_3/CNT film (e).

To identify the potential window of the asymmetric supercapacitor and balance the charges between the positive and negative electrodes, the electrochemical performance of the hybrid MnO_2/CNT and Fe_2O_3/CNT electrodes was investigated in a three-electrode system using platinum (Pt) foil, Ag/AgCl, and 1 M Na_2SO_4 aqueous solution as the counter electrode, reference electrode, and electrolyte, respectively. The MnO_2/CNT electrode shows a stable potential window of 0–1.2 V, while the Fe_2O_3/CNT electrode exhibits stable operation in the range of −0.8 to 0 V, indicating that the potential window of the assembled asymmetric supercapacitor can be potentially extended to 2 V, as shown in Fig. 2a. At a scan rate of 50 mV s^{-1}, the specific capacitance of the MnO_2/CNT positive electrode and Fe_2O_3/CNT negative electrode is 130.2 and 129.1 F g^{-1}, respectively. The charge balance between the two electrodes follows the relationship $Q_+ = Q_-$, in which the stored charge by each electrode is determined by the specific capacitance (C), the potential window (ΔU), and the mass (m) of each electrode using the following equation:

$$Q = C\Delta Um$$

Based on this calculation, the optimal mass ratio between the two electrodes should be around $m_{MnO_2/CNT}/m_{Fe_2O_3/CNT} = 0.66$.

Cyclic voltammetry (CV) curves of the ASS cell at 50 mV s^{-1} in different potential windows are displayed in Fig. 2b. Even when the potential window is increased up to 2 V, the rectangular shape of the CV curves with two weak symmetric broad redox peaks and the symmetric shape are maintained, indicating a good capacitive behaviour. The weak broad redox peaks are attributed to the pseudocapacitive behaviour of the supercapacitor resulting from the faradaic reactions of MnO_2 and Fe_2O_3. Fig. 2c shows the potential window dependence of the specific capacitance of the asymmetric supercapacitor. The specific capacitance increases significantly from 34 to 57.7 F g^{-1} with the operation potential from 0.8 to 2 V, meaning that the stored energy and delivered power can be improved at least by 961% according to the equation:

$$E = \frac{1}{2}CU^2.$$

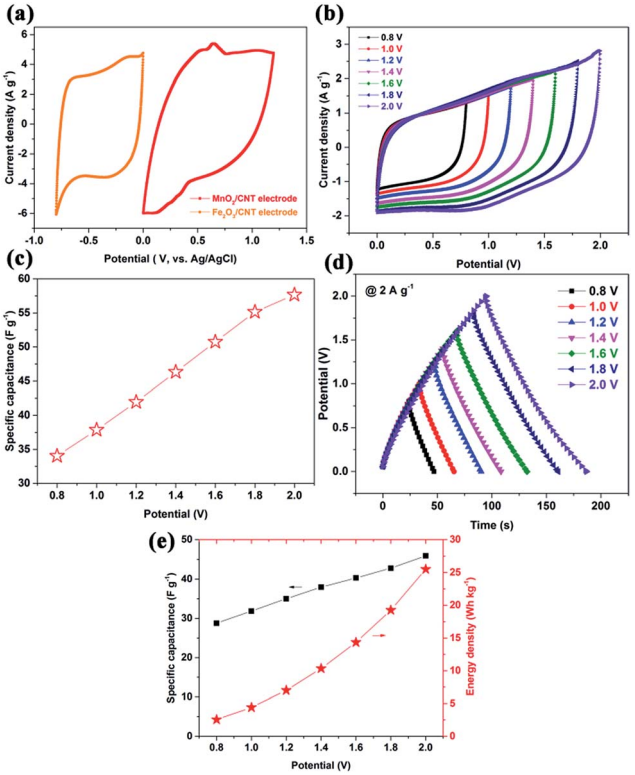

Fig. 2 (a) Comparative CV curves of MnO_2/CNT and Fe_2O_3/CNT electrodes recorded in a three-electrode cell in 1 M Na_2SO_4 aqueous solution at a scan rate of 50 mV s^{-1}. (b) CV curves of an optimized MnO_2/CNT and Fe_2O_3/CNT asymmetric supercapacitor recorded in different potential windows at a scan rate of 50 mV s^{-1}. (c) Specific capacitances of the ASS with the increase of the potential window in Na_2SO_4/PVA at a scan rate of 50 mV s^{-1}. (d) GCD curves obtained over different voltages from 0.8 to 2 V at a current density of 2 A g^{-1}. (e) Effects of the extended potential window on the specific capacitance and energy density.

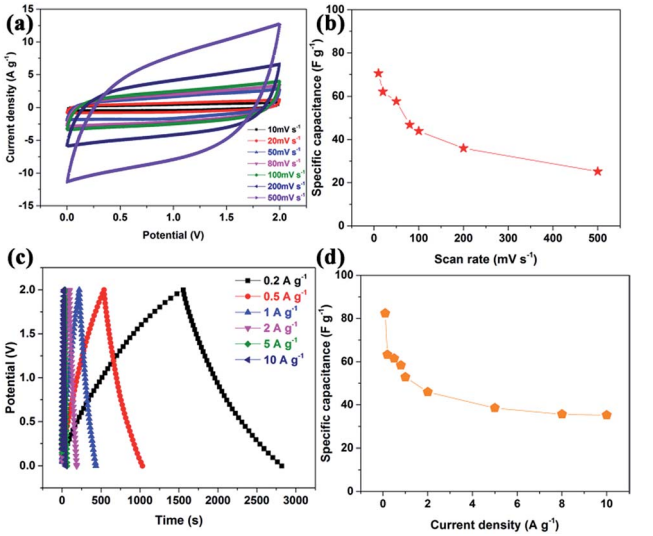

Fig. 3 (a) CV curves of an optimized ASS at scan rates ranging from 10 to 500 mV s^{-1}. (b) The scan rate dependence of specific capacitance. (c) GCD curves collected at different current densities for the ASS cell operated within a voltage window from 0 to 2 V. (d) Specific capacitance variation with current densities.

As a result, the overall performance of the supercapacitor is greatly improved. Note that operating at a higher voltage can provide additional advantages for practical applications, by reducing the number of devices in series required to reach a desired output voltage.

Similarly, galvanostatic charge–discharge (GCD) was also carried out at 2 A g^{-1} with different cell voltages from 0.8 to 2 V (Fig. 2d), and no overcharge curve was observed, inferring an excellent supercapacitor performance. The GCD result also shows an increase in charging and discharging time with increasing the cell voltage, thus indicating the increase of capacitance and energy density. These results also coincide with the CV results. Based on Fig. 2d, the effects of extending the potential window on specific capacitance and energy density are calculated and depicted in Fig. 2e. While the specific capacitance starts to increase slightly from 28.7 F g^{-1} at 0.8 V to 45.9 F g^{-1} at 2 V, the energy density increases significantly, ten-fold from 2.5 to 25.5 W h kg^{-1}, as the potential window is extended from 0.8 to 2 V.

Fig. 3a shows CV curves of an optimized ASS cell recorded at different scan rates of 10, 20, 50, 80, 100, 200, and 500 mV s^{-1} between 0 and 2 V. The CV profiles still retain a relatively rectangular shape without obvious distortion with increasing the scan rate, even at a high scan rate of 500 mV s^{-1}, indicating the desirable fast charge/discharge property for the power device. As shown in Fig. 3b, the specific capacitance gradually decreases with the increase of scan rates. It is understandable that at high scan rates, ionic diffusions of Na^+ ions and protons are most likely limited due to the time constraint, and only the outer active surface is utilized for the charge storage, resulting in a low electrochemical utilization of the electroactive materials. It is worth noting that the specific capacitance was calculated using the total mass of the two electrodes in the asymmetric supercapacitor, rather than a single electrode. More importantly, the maximum specific capacitance reaches 125.3 F g^{-1} at 1 mV s^{-1}, which is almost twice that of graphene//CNT asymmetric flexible supercapacitors[15] and CNT//CNT, MnO_2/CNT//MnO_2/CNT symmetrical stretchable or flexible supercapacitors.[5–7,9] The exceptional performances of the ASS cell are ascribed to the high capacitance and rate performance of both MnO_2/CNT and Fe_2O_3/CNT composites. Besides, the superior performance is further confirmed by GCD measurements at different current densities. As shown in Fig. 3c, the charge and discharge curves of the ASS device are reasonably symmetric. This further demonstrates the ideal capacitive characteristic and rapid charge–discharge property of the ASS cell. The specific capacitance calculated based on the discharge curves is 82.4 F g^{-1} (87% coulombic efficiency) at 100 mA g^{-1} (Fig. 3d), which is substantially higher than the values obtained from recent reports for other flexible supercapacitors.[15,20]

To demonstrate the stretchability of the ASS cell, a series of electrical and electrochemical tests were performed. Fig. 4a shows the normalized resistance at different strain levels, where R_0 is the resistance of the unstretched MnO_2/CNT electrode. Although the resistance of the Fe_2O_3/CNT electrode is ~15%

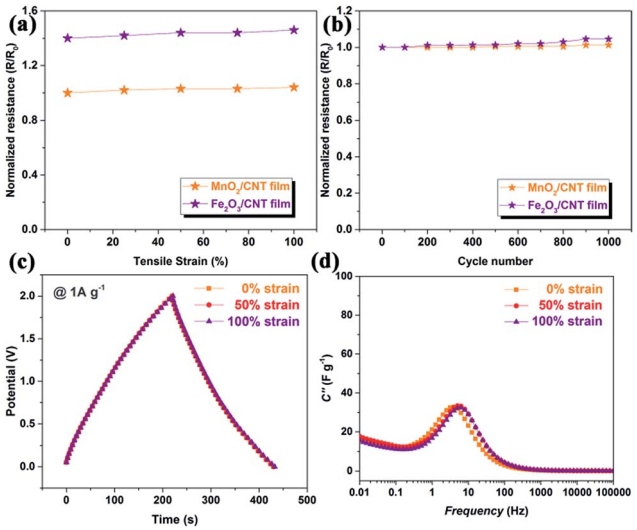

Fig. 4 (a) Normalized resistance *versus* tensile strain of wrinkled MnO_2/CNT and Fe_2O_3/CNT films subjected to tensile strains up to 100%. (b) Normalized resistance as a function of 1000 repeated stretching–releasing cycles between strains of 0 to 100%. (c) Comparison of GCD electrochemical performance of the ASS with 0, 50, and 100% strains at 1 A g^{-1}. (d) Bode plots of imaginary specific capacitance related to the relaxation time constant at 0, 50, and 100% strains.

higher than that of the MnO_2/CNT electrode, the conductivity of both MnO_2/CNT and Fe_2O_3/CNT electrodes did not vary much (less than 5%) with the increase of tensile strain up to 100%. In other words, without changing the original film length while stretching, the wrinkled MnO_2/CNT and Fe_2O_3/CNT films accommodate the applied tensile strains by just adjusting the buckling structure, resulting in nearly constant resistance.

The wrinkled MnO_2/CNT and Fe_2O_3/CNT composite films were further used to explore the resistance stability and mechanical durability during the mechanically dynamic processes between 0 and 100% strain, respectively. It should be noted that the resistance shows a small increment of <4% after 1000 dynamic stretching–releasing (DSR) cycles for both hybrid films subjected to a high strain rate of 10% strain per second (Fig. 4b), which demonstrates a superb mechanical robustness of the wrinkled MnO_2/CNT and Fe_2O_3/CNT films.

Similarly in the electrochemical performance of the ASS device, the slopes of discharge curves in Fig. 4c remain approximately constant as the supercapacitor deformed at different tensile strains (0%, 50%, and 100%), indicating a slight capacitance change. The excellent stretchability and electrochemical stability are due to the high interfacial strength to accommodate the various materials with different properties. Bode plots with imaginary specific capacitance deduced from the electrochemical impedance spectroscopy (EIS) data shown in Fig. 4d further explain the excellent stretchability and stability of the ASS cell. The equation below gives the imaginary parts of the specific capacitance:

$$C'' = \frac{Z'(\omega)}{m\omega|Z(\omega)|^2},$$

where C'' is the imaginary part of specific capacitance; Z' is the real part of impedance Z; m is the total mass of the electrode, and $\omega = 2\pi f$ is the radial frequency. The relaxation time constant $\tau^0(\tau^0 = {f_0}^{-1})$ is a quantitative measure of how fast a capacitor device could be charged and discharged reversibly and of practical importance in determining the rate at which the electrical response of a capacitor device can take place. The relaxation time constant from Fig. 4d in the frequency-dependent imaginary capacitance analysis quantitatively reveals its performance. From the C'' plot, it is observed that the overall frequency response of the cell from 0.01 Hz to 100 kHz in a relaxed and a stretched state is almost the same. The stable behaviour under the tensile strains from 0%, 50%, and 100% is in good agreement with the GCD results in Fig. 4c. τ^0 is less than 0.25 s at all strains. This extremely short relaxation time constant could be attributed to the outstanding conductivity of the CNT film, which facilitates MnO_2 and Fe_2O_3 redox reactions and leads to rapid capacitive behaviour. This extremely short relaxation time constant τ^0 at different strains also strongly suggests that the ASS device possesses tremendous potential for stable and instantaneous delivery of ultra-high power and energy under extreme mechanical deformation.

Long cycling life is an indispensable requirement for stretchable energy storage devices. The cycling life test for the ASS cell was carried out by repeating the GCD test between 0 and 2 V at a current density of 1 A g^{-1} for 10 000 cycles. Fig. 5a shows the capacitance retention of the ASS cell charged between 0 and 2 V as a function of the electrochemical cycle number. It is worth noting that the ASS cell is at 0% strain for the beginning 2000 GCD cycles and then strained to 100% from the 2001st cycle to the 8000th cycle, and finally at 50% strain for the rest

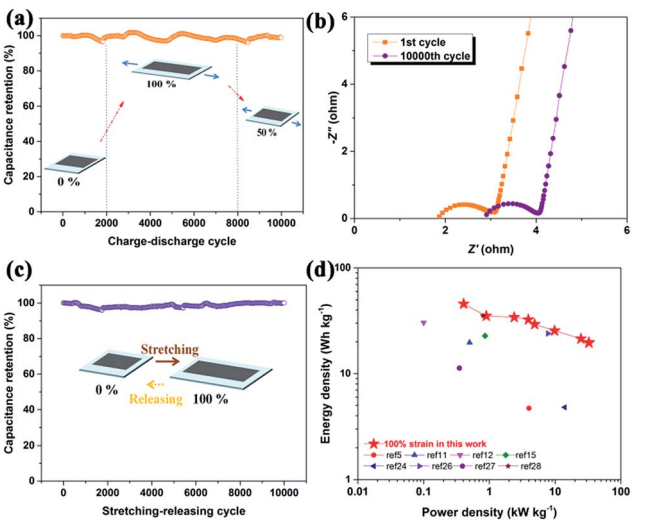

Fig. 5 (a) Long cycling stability of the ASS cell under 0%, 100%, and 50% strain at a constant current density of 1 A g^{-1} over 10 000 cycles. (b) Nyquist plots of the ASS cell in the frequency range of 100 kHz to 0.01 Hz recorded after the 1st and 10 000th cycle. (c) 10 000 mechanical stretching–releasing cycles between 0 and 100% strain at 10% strain per second at a current density of 1 A g^{-1}. (d) Ragone plot of the ASS at 100% strain and comparison with other flexible and stretchable asymmetric supercapacitors in the literature.

2000 GCD cycles. The ASS cell exhibits outstanding electrochemical stability with only 1.1% deterioration of the initial specific capacitance after 10 000 GCD cycles. Therefore, the retention of 98.9% after 10 000 cycles for the ASS is comparable to those of other recently reported asymmetric supercapacitors without any stretchability, such as graphene/MnO_2//activated carbon (AC) (97% retention after 1000 cycles),[21] MnO_2/graphene//graphene (79% retention after 1000 cycles),[12] and $Ni(OH)_2$//AC (94.3% retention after 3000 cycles).[17] These results further indicate that the ASS possesses not only exceptional electrochemical performance but also excellent stretchability.

The EIS analysis has been recognized as one of the principal methods for examining the fundamental behaviour of supercapacitors. For further understanding, the impedance of the asymmetric supercapacitor after the 1st and 10 000th cycle was measured in the frequency range of 100 kHz to 0.01 Hz at open circuit potential with an AC perturbation of 10 mV (Fig. 5b). After 10 000 cycles, nearly no change is observed for R_{ct} (1.1 Ω), and only a slight increase of R_s from 1.9 to 2.9 Ω is observed. These EIS results further demonstrate the exceptional electrochemical stability of the ASS cell.

The ASS can also be expected to accommodate volumetric expansion of MnO_2 and Fe_2O_3 during charge–discharge cycles due to the highly conductive nature of the CNT framework in the composites. However, the volumetric expansion effect can be further enlarged during stretching and releasing when a portion of the MnO_2 and Fe_2O_3 nanoparticles will have the potential to migrate more easily with dynamic mechanical shock. This was verified by testing the attainable mechanical stretching–releasing cycles, which reveal device durability for practical applications and are also very critical in addition to evaluating their long GCD cycling stability. The ASS cell was tested for 10 000 DSR cycles with a strain rate of 10% per second at a constant current density of 1 A g^{-1}. Fig. 5c shows that the capacitance retention is extremely high where the capacitance fades by merely less than 1%, further proving the excellent durability of the ASS cell from the mechanical viewpoint. It is apparent that MnO_2 and Fe_2O_3 nanoparticles are still firmly anchored on the surface of CNTs and agglomerated at the crossing of nanotubes, although they experience the volumetric variations generated by the electrochemical processes and the mechanical shock at the same time. Such good cycle performance is comparable with that of other stretchable supercapacitors and is highly promising for practical applications.[3,5–10]

The energy density reaches 45.8 W h kg^{-1} at a power density of 406.6 W kg^{-1} and remains at 19.6 W h kg^{-1} at a power density of 32.7 kW kg^{-1} (Fig. 5d). The specific energy density values achieved with a cell voltage of 2 V in this work are much higher than those of recently reported flexible/stretchable symmetrical CNT//CNT supercapacitors (<12.5 W h kg^{-1}),[5–7,22] graphene//graphene supercapacitors (<26 W h kg^{-1}),[23] MnO_2//MnO_2 supercapacitors (<4.8 W h kg^{-1}),[24] and polypyrrole/CNT supercapacitors (<32.7 W h kg^{-1}).[25] It is also better than that of existing asymmetric flexible supercapacitors with an aqueous electrolyte, such as RuO_2/graphene//graphene (19.7 W h kg^{-1}),[11] MnO_2/graphene//graphene (30.4 W h kg^{-1}),[12] MnO_2/CNT//CNT (6.0 W h kg^{-1}),[15] graphene/MnO_2/CNT//AC/CNT (24 W h kg^{-1}),[26] Bi_2O_3//MnO_2 (11.3 W h kg^{-1}),[27] and Co_2AlO_4@MnO_2//Fe_3O_4 (35.2 W h kg^{-1}).[28] Thus, it is obvious that the as-assembled MnO_2/CNT//Fe_2O_3/CNT asymmetric stretchable supercapacitor displays excellent energy performance and shows attractive potential for practical applications.[29–39] The superior electrochemical performance of the ASS can be attributed to the following aspects: (1) The CNT films in the composites assist in maintaining mechanical integrity and high electrical conductivity of the overall electrodes due to their superior mechanical properties, good electrochemical stability, and excellent conductivity. (2) Well-dispersed MnO_2 nanoparticles can greatly shorten the diffusion and migration paths of electrolyte ions during the rapid charge–discharge process; accordingly, high electrochemical utilization of MnO_2 is ensured. (3) The carbon-based anodes usually limit the energy density of the asymmetric supercapacitors due to their relatively lower specific capacitance. The present Fe_2O_3/CNT composite exhibits greatly improved specific capacitance due to the synergetic effect of highly conductive CNTs providing fast electron transfer and large surface area and well-dispersed Fe_2O_3 nanoparticles contributing large pseudocapacitance. The large specific capacitance of the present Fe_2O_3/CNT composite is comparable with that of the MnO_2/CNT composite, making the desirable anode–cathode coupling build a 2 V asymmetric supercapacitor with both high energy density and power density. (4) The binder-free device fabrication provides a low interfacial resistance and fast electrochemical reaction rate.

Conclusions

In conclusion, an all-solid-state asymmetric stretchable supercapacitor based on the MnO_2/CNT hybrid film positive electrode, the Fe_2O_3/CNT composite film negative electrode, and the solid state Na_2SO_4/PVA gel electrolyte was fabricated. Due to the good conductivity of the CNT films and the extended potential window of 2 V, the specific capacitance and the energy density were greatly enhanced. In addition to its excellent electrochemical performance, the remarkable stretchability of up to 100% tensile strain made this supercapacitor a promising energy storage device for practical applications. The asymmetric configuration has been demonstrated to be the preferable stretchable supercapacitor structure to achieve a higher operating voltage and high energy density without sacrificing the power delivery and cycle stability.

Experimental section

Preparation of Fe_2O_3/CNT and MnO_2/CNT films

CNT films were prepared using a modified floating chemical vapour deposition method according to previously published work.[40] Briefly, the precursor, a mixture of ferrocene and sulfur (atomic ratio Fe : S = 1 : 10, both from Sigma-Aldrich), was heated to 1150 °C in a tube furnace with a mixed gas flow of Ar (1500 mL min^{-1}) and H_2 (150 mL min^{-1}). After 30 min of reaction, the as-obtained unpurified CNT films were transferred into a ceramic cubicle to be heat-treated at 450 °C in air for 30 min. The samples were then cooled down, and the

Fe_2O_3/CNT films were obtained.[41] Some of the Fe_2O_3/CNT films were then immersed in concentrated HCl (37% by volume percent) for 72 h to remove the Fe_2O_3 oxidized from Fe catalysts during the heat treatment. Then the films were rinsed with deionized (DI) water until the pH became neutral. The freestanding films were held up on a frame made of stainless steel and dried at room temperature (RT) overnight. The MnO_2/CNT film electrodes were then prepared by modified precipitation.[42] Briefly, the purified CNT film as above was immersed in ethanol while 0.1 M $KMnO_4$ aqueous solution was added drop-wise. A thin layer of nanostructured MnO_2 was deposited on the surface of the CNT bundles with 30 min precipitation time. The resulting MnO_2/CNT electrodes were rinsed excessively in deionized water and ethanol and finally dried at room temperature for 24 h.

Preparation of the gel electrolyte

Na_2SO_4 (1 M, 6 g) and PVA powder (6 g, Sigma Aldrich, M_w = 89 000 to 98 000) were added into 60 mL of deionized water, which were heated to 85 °C under stirring until the mixture became clear.

Assembly of asymmetric stretchable supercapacitors

The as-prepared Fe_2O_3/CNT and MnO_2/CNT films were laminated tightly with a UV-light treated PDMS substrate. The stretchable electrodes were then stretched to 100% strain. Subsequently, the liquid Na_2SO_4/PVA gel electrolyte was coated on the surface of electrodes by means of dip coating, leaving the uncoated part to be connected to current collectors. After the electrolyte had solidified, one MnO_2/CNT and the other Fe_2O_3/CNT film were stacked together with the electrolyte-coated parts overlapping with each other. The electrical resistance between them was monitored using a multimeter to avoid a short circuit. The assembled ASS was placed in a fume hood under ambient conditions to allow the gel electrolyte to solidify.

Characterization

The morphology and structure were characterized using a Zeiss Auriga 60 FIB/SEM. The mass of the freestanding electrode was weighed using a micro/ultramicro-balance (Mettler Toledo XP6) with 0.001 mg accuracy. The galvanostatic discharge–charge tests were carried out on four-channel battery testing equipment (Arbin Instrument, Ltd.). Electrochemical impedance spectroscopy was performed on a PARSTAT 2273 potentiostat/galvanostat (Princeton Applied Research) with 10 mV amplitude of AC signals from 100 kHz to 10 mHz. Cyclic voltammetry measurements were also obtained using the electrochemical workstation (Princeton Applied Research). The dynamic electrochemical measurements were performed while the ASS was being stretched and released between 0% and 100% tensile strains.

Calculation

The specific capacitance of the ASS was calculated based on the total mass of both positive and negative electrodes (0.33 mg). The energy and power densities were calculated by conducting GCD cycling with different constant current densities from the slope of the discharge capacitance. The frequency dependence of the imaginary part (C'') of electrochemical capacitance was obtained from EIS measurements.

Notes and references

1 J. A. Rogers, T. Someya and Y. Huang, *Science*, 2010, **327**, 1603–1607.
2 D.-H. Kim, R. Ghaffari, N. Lu and J. A. Rogers, *Annu. Rev. Biomed. Eng.*, 2012, **14**, 113–128.
3 K. Xie and B. Wei, *Adv. Mater.*, 2014, **26**, 3592–3617.
4 R. Bondade, Y. Zhang, B. Wei, T. Gu, H. Chen and D. Ma, *IEEE Trans. Ind. Electron.*, 2016, **63**, 1.
5 C. Yu, C. Masarapu, J. Rong, B. Wei and H. Jiang, *Adv. Mater.*, 2009, **21**, 4793–4797.
6 X. Li, T. Gu and B. Wei, *Nano Lett.*, 2012, **12**, 6366–6371.
7 Z. Niu, H. Dong, B. Zhu, J. Li, H. H. Hng, W. Zhou, X. Chen and S. Xie, *Adv. Mater.*, 2013, **25**, 1058–1064.
8 P. Xu, T. Gu, Z. Cao, B. Wei, J. Yu, F. Li, J.-H. Byun, W. Lu, Q. Li and T.-W. Chou, *Adv. Energy Mater.*, 2014, **4**, 1300759.
9 T. Gu and B. Wei, *Nanoscale*, 2015, 11626–11632.
10 S. Xu, Y. Zhang, J. Cho, J. Lee, X. Huang, L. Jia, J. A. Fan, Y. Su, J. Su, H. Zhang, H. Cheng, B. Lu, C. Yu, C. Chuang, T.-I. Kim, T. Song, K. Shigeta, S. Kang, C. Dagdeviren, I. Petrov, P. V. Braun, Y. Huang, U. Paik and J. A. Rogers, *Nat. Commun.*, 2013, **4**, 1543.
11 B. G. Choi, S.-J. Chang, H.-W. Kang, C. P. Park, H. J. Kim, W. H. Hong, S. Lee and Y. S. Huh, *Nanoscale*, 2012, **4**, 4983.
12 Z. S. Wu, W. Ren, D. W. Wang, F. Li, B. Liu and H. M. Cheng, *ACS Nano*, 2010, **4**, 5835–5842.
13 Y. J. Kang, H. Chung and W. Kim, *Synth. Met.*, 2013, **166**, 40–44.
14 Z. Lei, J. Zhang and X. S. Zhao, *J. Mater. Chem.*, 2012, **22**, 153.
15 J. Liu, L. Zhang, H. Bin Wu, J. Lin, Z. Shen and X. W. Lou, *Energy Environ. Sci.*, 2014, **7**, 3709–3719.
16 H. Wang, Y. Liang, T. Mirfakhrai, Z. Chen, H. S. Casalongue and H. Dai, *Nano Res.*, 2011, **4**, 729–736.
17 J. Yan, Z. Fan, W. Sun, G. Ning, T. Wei, Q. Zhang, R. Zhang, L. Zhi and F. Wei, *Adv. Funct. Mater.*, 2012, **22**, 2632–2641.
18 W. Wei, X. Cui, W. Chen and D. G. Ivey, *Chem. Soc. Rev.*, 2011, **40**, 1697–1721.
19 Q. Qu, S. Yang and X. Feng, *Adv. Mater.*, 2011, **23**, 5574–5580.
20 Y. He, W. Chen, X. Li, Z. Zhang, J. Fu, C. Zhao and E. Xie, *ACS Nano*, 2013, **7**, 174–182.
21 Z. Fan, J. Yan, T. Wei, L. Zhi, G. Ning, T. Li and F. Wei, *Adv. Funct. Mater.*, 2011, **21**, 2366–2375.
22 M. Kaempgen, C. K. Chan, J. Ma, Y. Cui and G. Gruner, *Nano Lett.*, 2009, **9**, 1872–1876.
23 J. Zang, C. Cao, Y. Feng, J. Liu and X. Zhao, *Sci. Rep.*, 2014, **4**, 6492.
24 L. Yuan, X.-H. Lu, X. Xiao, T. Zhai, J. Dai, F. Zhang, B. Hu, X. Wang, L. Gong, J. Chen, C. Hu, Y. Tong, J. Zhou and Z. L. Wang, *ACS Nano*, 2012, **6**, 656–661.
25 K. Liang, T. Gu, Z. Cao, X. Tang, W. Hu and B. Wei, *Nano Energy*, 2014, **9**, 245–251.

26 Y. Cheng, H. Zhang, S. Lu, C. V. Varanasi and J. Liu, *Nanoscale*, 2013, **5**, 1067–1073.
27 H. Xu, X. Hu, H. Yang, Y. Sun, C. Hu and Y. Huang, *Adv. Energy Mater.*, 2015, **5**, 1–7.
28 F. Li, H. Chen, X. Y. Liu, S. J. Zhu, J. Q. Jia, C. H. Xu, F. Dong, Z. Q. Wen and Y. X. Zhang, *J. Mater. Chem. A*, 2016, **4**, 2096–2104.
29 B. You, L. Wang, L. Yao and J. Yang, *Chem. Commun.*, 2013, **49**, 5016–5018.
30 B. You, N. Jiang, M. Sheng and Y. Sun, *Chem. Commun.*, 2015, **4252**, 4252–4255.
31 B. You, N. Li, H. Zhu, X. Zhu and J. Yang, *ChemSusChem*, 2013, **6**, 474–480.
32 H. Bin Wu, G. Zhang, L. Yu and X. W. Lou, *Nanoscale Horiz.*, 2016, **1**, 27–40.
33 B. You, P. Yin and L. An, *Small*, 2014, **10**, 4352–4361.
34 L. Li, S. Peng, H. Bin Wu, L. Yu, S. Madhavi and X. W. Lou, *Adv. Energy Mater.*, 2015, **5**, 1500753.
35 B. You, F. Kang, P. Yin and Q. Zhang, *Carbon*, 2016, **103**, 9–15.
36 K. Liang, N. Wang, M. Zhou, Z. Cao, T. Gu, Q. Zhang, X. Tang, W. Hu and B. Wei, *J. Mater. Chem. A*, 2013, **1**, 9730.
37 Q. Qu, P. Zhang, B. Wang, Y. Chen, S. Tian, Y. Wu and R. Holze, *J. Phys. Chem. C*, 2009, **113**, 14020–14027.
38 T. Brousse, M. Toupin, R. Dugas, L. Athouël, O. Crosnier and D. Bélanger, *J. Electrochem. Soc.*, 2006, **153**, A2171.
39 V. Subramanian, H. Zhu, R. Vajtai, P. M. Ajayan and B. Wei, *J. Phys. Chem. B*, 2005, **109**, 20207–20214.
40 H. Zhu and B. Wei, *Chem. Commun.*, 2007, 3042–3044.
41 Z. Cao and B. Wei, *J. Power Sources*, 2013, **241**, 330–340.
42 X. Li and B. Wei, *Nano Energy*, 2012, **1**, 479–487.